

A&A manuscript no. (will be inserted by hand later)	ASTRONOMY AND ASTROPHYSICS 13.10.2018
Your thesaurus codes are: 03(11.09.1 UGC 10205; 11.11.1; 11.19.2; 11.19.6)	

Figure-of-eight velocity curves: UGC 10205^{*}

J.C. Vega¹, E.M. Corsini², A. Pizzella², and F. Bertola²

¹ Telescopio Nazionale Galileo, Osservatorio Astronomico di Padova, vicolo dell'Osservatorio 5, I-35122 Padova, Italy

² Dipartimento di Astronomia, Università di Padova, vicolo dell'Osservatorio 5, I-35122 Padova, Italy

Received.....; accepted.....

Abstract. We measured the velocity curve and the velocity dispersion profile of the ionized gas along the major axis of the edge-on galaxy UGC 10205. The observed kinematics extends up to about 40'' from the nucleus. In the inner $\pm 13''$ of this early-type spiral three kinematically distinct gaseous components are present. We disentangle a fast-rotating and a slow-rotating component. They give to the UGC 10205 velocity curve a “figure-of-eight” appearance. A third velocity component is also detected on the southeast side of the galaxy. Possibly it is produced by gas in non-circular motions.

Key words: galaxies: individual: UGC 10205 — galaxies: kinematics and dynamics — galaxies: spiral — galaxies: structure

1. Introduction

Within the last year ionized gas kinematics has revealed in a number of edge-on disk galaxies double-peaked emission lines. The analysis of the line profiles allows to derive individual rotation curves characteristic of two kinematically distinct gas components.

The edge-on S0 galaxy NGC 7332 has been found to have an “x-shaped” velocity curve, indicating two gas components counterrotating one with respect to the other (Plana &

Send offprint requests to: J.C. Vega;
jvega@astrpd.pd.astro.it

^{*} Based on observations carried out at the INT operated on the island La Palma by the Royal Greenwich Observatory in the Spanish Observatorio del Roque de Los Muchachos of the Instituto de Astrofísica de Canarias, Tenerife, Spain.

Boulesteix 1996).

In the inner regions of the Sc NGC 5907 Miller & Rubin (1995) observed double-valued ionized gas emissions. They attributed the higher velocity system to disk gas near the nucleus, and the lower velocity system to an outer gas ring. Although these two gas components are supposed to be spatially distinct, they are viewed superimposed along the line-of-sight on account of NGC 5907 high inclination.

The spirals NGC 5746 (Kuijken & Merrifield 1995; Bureau & Freeman 1996), NGC 5965 (Kuijken & Merrifield 1995), IC 5096 (Bureau & Freeman 1996) and NGC 2683 (Merrifield 1996) have boxy/peanut bulges and double-peaked gas line profiles. Kuijken & Merrifield (1995) explained these features as the signature of a disk non-axisymmetric potential due to the presence of a bar.

In this paper we show yet an other case of edge-on disk galaxy with a multiple-valued gas velocity curve, namely UGC 10205. For projected distances lower than 13'' from the nucleus UGC 10205 it is characterized by the presence of three kinematically distinct gaseous components, two of which give to its velocity curve a “figure-of-eight” appearance. UGC 10205 is classified as Sa spiral by Nilson (1973) and by de Vaucouleurs et al. (1991). Its total *B*-band magnitude is $B_T = 14.4$ mag (RC3) and the inclination of the galaxy deduced from the disk parameters is $i = 84^\circ$ (Rubin et al. 1985). The distance is 132 Mpc ($H_0 = 50 \text{ km s}^{-1} \text{ Mpc}^{-1}$).

2. Observations and data reduction

The spectroscopic observations of UGC 10205 were carried out on March 19-21, 1996 at the Isaac Newton Telescope (INT) in La Palma us-

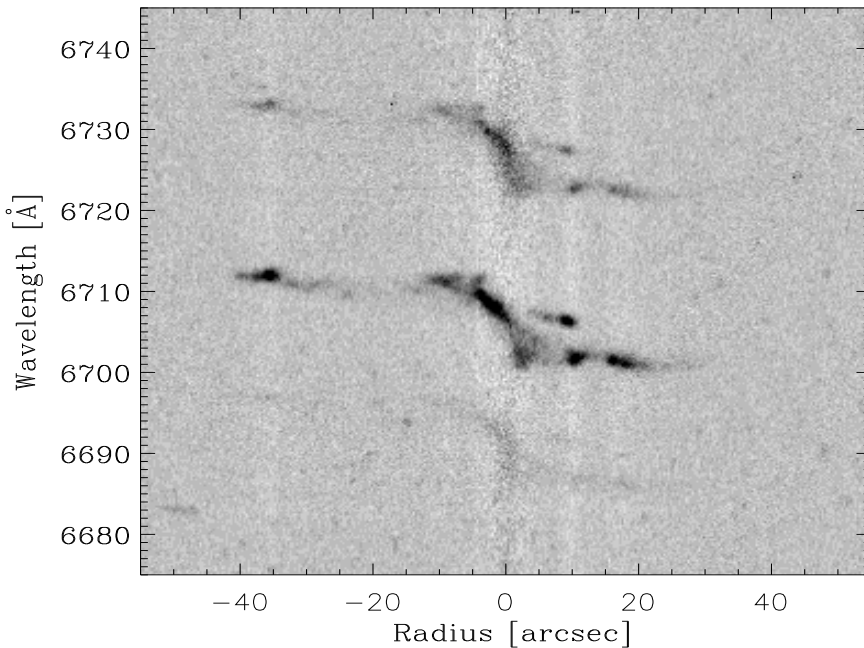


Fig. 1. UGC 10205 major axis 100 minutes spectrum in the $H\alpha$ region after removal of sky and stellar continuum. Note the multiple-peaked emissions of the $H\alpha$ and the $[N\text{ II}]$ ($\lambda 6583.4$ Å) lines in the central regions of the spectrum ($|r| \leq 13''$)

ing the Intermediate Dispersion Spectrograph (IDS).

The H1800V grating with 1800 grooves mm^{-1} was used in the first order in combination with a $1.9'' \times 4.0'$ slit, the 500 mm camera and the AgRed collimator. It yielded a wavelength coverage of ~ 240 Å between 6650 Å and 6890 Å with a reciprocal dispersion of 9.92 Å mm^{-1} . We checked that the measured FWHMs do not depend on wavelength and we found a mean value of $\text{FWHM} = 0.86$ Å (i.e. $\sigma = 0.37$ Å) that, in the range of the observed gas emission lines, corresponds to ~ 17 km s^{-1} . No on-chip binning was done on the adopted 1024×1024 TK1024A CCD. Each $24 \mu\text{m} \times 24 \mu\text{m}$ image pixel corresponds to 0.24 Å \times $0.33''$.

We took two separate major axis spectra (P.A. = 132°) for a total exposure time of 100 minutes (Fig. 1). The slit was centered visually on the galaxy nucleus. A comparison copper-argon lamp exposure was obtained between the two object integrations. All the images were reduced using standard MIDAS routines. Considering a sample of 8 bright OH night-sky emission lines, we found a mean deviation from the theoretical predicted wavelength (Osterbrock & Martel, 1992) corresponding to ~ 1 km s^{-1} .

The gas velocities and velocity dispersions for $|r| > 13''$, where the ionized gas emission

lines have a Gaussian profile shape, were derived by means of the MIDAS package ALICE. We measured the $H\alpha$ and the $[N\text{ II}]$ ($\lambda 6583.4$ Å) lines, where they were clearly detected. The position, the FWHM and the uncalibrated flux of each emission line were individually determined by interactively fitting one Gaussian plus a polynomial to each emission and to its surrounding continuum. The wavelength of the Gaussian center was converted to the velocity $v = cz$, and then a heliocentric correction of $\Delta v = +15.5$ km s^{-1} was applied. The Gaussian FWHM was corrected for the instrumental FWHM and then converted to the velocity dispersion σ . The ionized gas emission lines are double-peaked for $-13'' \leq r < 3''$ and even triple-peaked for $3'' \leq r \leq 13''$. They have been fitted using the above package with two or three Gaussians respectively and a polynomial continuum. At each radius this multiple-Gaussian fit has been done separately for each emission line.

The gas velocity curves and the velocity dispersion profiles independently derived from the $H\alpha$ (Fig. 2) and the $[N\text{ II}]$ (Fig. 3) lines are in good agreement at all radii. The kinematical data from $H\alpha$ and $[N\text{ II}]$ lines are given in Table 1 and in Table 2 respectively. Each table provides the radial distance from the galaxy center r in arcsec (col. 1), the observed heliocentric velocity v (col. 2) and the velocity dis-

persion σ (col. 3) in km s^{-1} , the number n of spectrum rows binned along the spatial direction to improve the signal-to-noise ratio of the emission lines (col. 4) and the identification i of the kinematically distinct gas components (col. 5).

3. Results

The observed gas kinematics extends out to $42''$ (~ 27 kpc) in the receding NW side and about up to $30''$ (~ 19 kpc) in the SE approaching side respectively.

For $|r| \leq 13''$ (~ 8 kpc) we are able to disentangle (Fig. 1 and Fig. 2) three kinematically distinct gaseous components, named as fast-rotating (i), slow-rotating (ii) and third (iii). The fast-rotating gas component (i) shows a velocity curve with a very steep gradient, reaching an observed maximum rotation of 240 km s^{-1} at $|r| \sim 3''$ (~ 2 kpc) from the center and remaining almost constant for $|r| > 3''$. Its velocity dispersion has a central peak of about 90 km s^{-1} and it shows a sharp decrease to values lower than 25 km s^{-1} outwards. The radial velocity of the slow-rotating gas component (ii) increases linearly with the distance from the galaxy center reaching 240 km s^{-1} at $|r| \sim 14''$ (~ 9 kpc). The velocity dispersion remains between 40 km s^{-1} and 50 km s^{-1} . This range is larger in the [N II] line, which however is characterized by a lower signal-to-noise ratio. In the radial range between $r \sim 3''$ and $r \sim 13''$ along the SE side of the major axis the $\text{H}\alpha$ and [N II] emissions have triple-peaked lines. Indeed in this region the component (iii) is observed. It has a radial velocity increasing linearly from $v \sim 6551 \text{ km s}^{-1}$ to $v \sim 6611 \text{ km s}^{-1}$ and equal to the systemic velocity at $r \sim 8''$ (~ 5 kpc). It has a quite low velocity dispersion of $\sigma \sim 15 \text{ km s}^{-1}$. For $|r| > 13''$ a single-valued velocity curve is measured, showing the tendency to flatten out. The velocity dispersions in this radial range are lower than 30 km s^{-1} .

Adopting the center of symmetry of velocities for $|r| \leq 13''$ as the systemic heliocentric velocity, we derived $V_{\odot} = 6583 \pm 5 \text{ km s}^{-1}$ in agreement with $V_{\odot} = 6581 \pm 15 \text{ km s}^{-1}$ found by Rubin et al. (1985).

Studying the ionized gas velocity curves of a sample of Sa spirals, also Rubin et al. (1985) noticed along the SE side of the UGC 10205 major axis “a curious three-velocity system” within 10 kpc of the center. It can not be reconciled with our component (i), (ii), and (iii).

The reciprocal dispersion (25 \AA mm^{-1}) and the spatial scale ($25'' \text{ mm}^{-1}$) of their image-tube spectrum were respectively 3 and 2 times lower than those of our CCD spectrum. So they did not disentangle the component (i) from the (ii), detecting them as a unique one. They observed a second velocity system, corresponding to velocity curve of component (iii). Finally, for two distinct radii at $r \sim -5''$ they measured intermediate velocities between those of the first and the second system and considered them as related to a third velocity component.

4. Discussion

In the inner $\pm 13''$ UGC 10205 we are facing two main kinematically distinct gaseous components, namely (i) and (ii). They have quite similar velocity dispersion profiles but very different velocity curves, which produce the “figure-of-eight” appearance of UGC 10205 velocity curve.

What is the real spatial distribution of these two components? Are they really cospatial or are they spatially distinct and seen superimposed on account of a projection effect?

The simultaneous presence of the two gas components at the same distance of the galaxy center raises the problem of the viscous interaction of distinct gaseous structures with different kinematical characteristics. One possibility is the gas to be distributed in collisionless cloudlets, as suggested by Cinzano & van der Marel (1994) to explain the ionized gas kinematics in the E4 NGC 2974. If this is the case, we would expect the slow-rotating component being supported by a velocity dispersion higher than that we observed.

We are left with the interpretation already given by Miller & Rubin (1995) for NGC 5907 and by Kuijken & Merrifield (1995) for NGC 5746 and NGC 5965 that the two gas components are spatially distinct and viewed superimposed along the line-of-sight due to the high inclination of the galaxy. The linear rise of the velocity curve of component (ii) up to the points of conjunction with those of component (i) is due to the so-called “rim of the wheel” effect when viewing at an enhanced ring structure. Moreover, the radial trend of line intensity derived for the two components seem to confirm this interpretation. Indeed, the intensity of component (i) is peaked in the center, while the intensity of component (ii) is

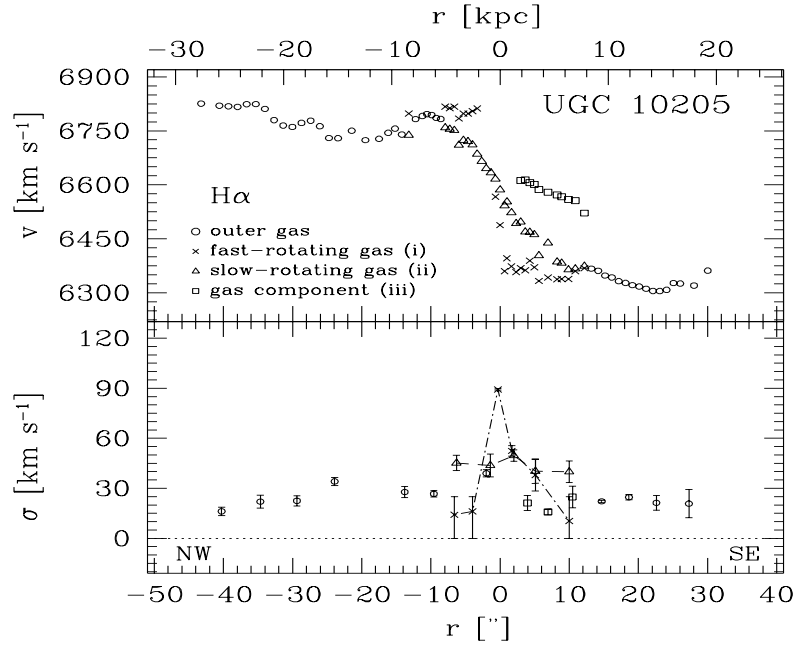


Fig. 2. UGC 10205 major-axis $H\alpha$ kinematics: observed heliocentric velocity curve (top) and velocity dispersion profile (bottom) of the gaseous fast-rotating (*crosses*), slow-rotating (*open triangles*), and third (*open squares*) component. The *open circles* are used where $H\alpha$ was fitted using a single Gaussian. The velocity dispersion σ is plotted with a different spatial binning than v . The *dash-dotted* and the *short-dashed* lines connect σ values of the fast and the slow-rotating components respectively

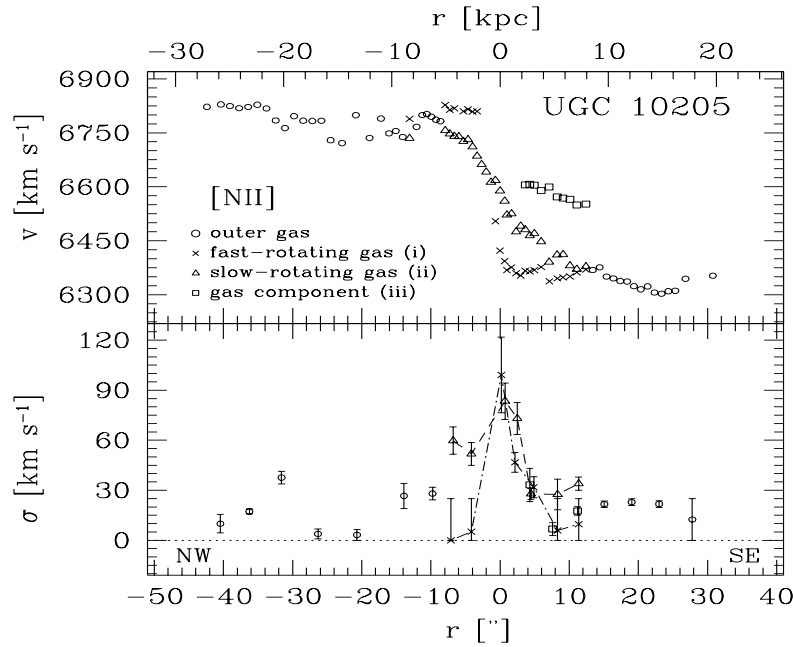


Fig. 3. Same as Fig. 2 for the $[N\ II]$ ($\lambda 6583.4\ \text{\AA}$) emission line

almost constant as we are expecting if component (ii) is actually an outer ring.

The above gas configuration is the one expected in a barred galaxy. Indeed the bar exerts a torque on the disk gas, which is slowly drifted from the regions around the corotation radius towards the Lindblad resonances to form rings. Kuijken & Merrifield (1995) and Merrifield (1996) showed the line-of-sight velocity distribution (LOSVD) in function of the projected radius for the closed non-intersecting orbits allowed by a barred disk potential in edge-on galaxies. (Due to its collisional nature, the gas moves only onto the closed non-intersecting orbits.) They found the LOSVDs with the characteristic “figure-of-eight” variation with radius. For this reason they considered the gaps in such LOSVDs as the signature of the presence in the disk of the gas-depleted regions due to the bar. The gas components (ii) in the velocity curve of UGC 10205 is produced by the ring formed at the outer Lindblad resonance.

The third gas component observed in the inner regions of UGC 10205 is very peculiar. It is present only on the SE side and it has a velocity ranging from $\sim -30 \text{ km s}^{-1}$ to $\sim +30 \text{ km s}^{-1}$ if reported to the systemic velocity of the galaxy. So it is not moving around the galaxy center in circular orbits. It could be associated to the faint features embedding UGC 10205 and visible in the R -band images shown by Rubin (1987). Its kinematics can be explained if such gas moves onto an elliptical orbit, which at the projected distance of $r \sim 8''$ has its tangent perpendicular to the line-of-sight. The gas of component (iii) populates only a portion of this orbit. From the available data we can not infer the proper distance of component (iii) from the galaxy center.

Outside $13''$ we observe single-peaked emission lines produced by disk gas in near-circular motion. For radial distances greater than that of the outer Lindblad resonance we expect the gas to be only little disturbed by the inner triaxial potential. Because of the edge-on orientation of the disk with respect to the line-of-sight, if the gas is distributed uniformly decreasing throughout the disk we would expect to observe emission lines peaked at the local circular velocity with an asymmetry towards the lower velocities. This emission feature is present in UGC 10205 in the form of very low luminous intensity. It is superimposed to a major emission that does not show any systematic

deviation from the Gaussian shape. Irregularities in the velocity curve can be easily produced by the fact of the integration along the line-of-sight being the galaxy seen on edge.

The interpretation of Kuijken & Merrifield (1995) has been recently adopted by Merrifield (1996) for NGC 2683 observed by Rubin, and by Bureau & Freeman (1996) for IC 5096. It could also be applied not only to UGC 10205 but also to the case NGC 5907, extending the explanation given by Miller & Rubin (1995). Since their two spirals have peanut-shaped bulges, Merrifield and Kuijken (1995) suggested a connection between the peanut bulges, which are detectable only in edge-on galaxies, and the bars, which are easily detectable in more face-on systems. Anyway, while NGC 2683, NGC 5746, NGC 5965 and IC 5096 have boxy/peanut-shape bulges, for NGC 5907 and UGC 10205 this crucial photometric information is still not available.

The presence of the “figure-of-eight” in gas velocity curves of edge-on spirals seems to be unrelated to the morphological type in the spiral sequence since in RC3 UGC 10205 is classified Sa, NGC 2683, NGC 5746 and NGC 5965 are Sb, IC 5096 is Sbc, and NGC 5907 is Sc.

The geometrical distribution of the gas giving rise to the “figure-of-eight” velocity curves could be used in the interpretation of phenomena like the one described by Plana & Boulesteix (1996) in the S0 NGC 7332. It is an edge-on galaxy with a boxy-shaped bulge (Fisher & Illingworth 1994). Plana & Boulesteix (1996) separated clearly two extended coplanar counterrotating components of ionized gas, which were previously detected by Fisher & Illingworth (1994). One of these components has a linearly increasing velocity curve (“rim of the wheel” effect). If we imagine to invert the sense of rotation of this latter component, a typical “figure-of-eight” velocity curve is obtained. Therefore a gas distribution like that of the above-mentioned edge-on barred spirals but with an outer ring counterrotating with respect to the inner gas could reproduce the kinematics of NGC 7332, for which a satisfactory interpretation has been not given. Of course, theoretical modelling should justify this situation.

Acknowledgements. We thank M.R. Merrifield for useful discussion. AP acknowledges support from an *Acciaierie Beltrame* grant.

References

- Bureau, M., & Freeman, K. C. 1996, in “The Nature of Elliptical Galaxies”, Proc. 2nd Stromlo Symp., eds. M. Arnaboldi, G. S. Da Costa & P. Saha, in press
- Cinzano, P., & van der Marel, R.P. 1994, MNRAS, 270, 325
- de Vaucouleurs, G., de Vaucouleurs, A., Corwin, H. G. Jr., Buta, R. J., Paturel, G., & Fouqu e, P. 1991, Third Reference Catalogue of Bright Galaxies. Springer-Verlag, New York (RC3)
- Fisher, D., & Illingworth, G. 1994, AJ, 107, 160
- Kuijken, K., & Merrifield, M. R. 1995, ApJ, 443, L13
- Merrifield, M. R. 1996, in “Barred Galaxies”, ASP Conf. Ser. Vol. 91, eds. R. Buta, D. A. Crocker & B. G. Elmegreen, p.179
- Miller, B. W., & Rubin, V. C. 1995, AJ, 110, 2692
- Nilson, P. 1973, Uppsala General Catalogue of Galaxies. Uppsala Astronomical Observatory, Uppsala
- Osterbrock, D. E., & Martel, A. 1992, PASP, 104, 76
- Plana, H., & Boulesteix, J. 1996, A&A, 307, 391
- Rubin, V. C. 1987, in “Dark Matter in the Universe”, IAU Symp. No. 117, eds. J. Kormendy & G. R. Knapp, p. 51
- Rubin, V. C., Burstein, D., Ford, Jr., W.K., & Thonnard, N. 1985, ApJ, 289, 81

Table 1. UGC 10205 major axis H α kinematics

r	v	σ	n	i^a	r	v	σ	n	i^a
(1)	(2)	(3)	(4)	(5)	(1)	(2)	(3)	(4)	(5)
-43.2	6826	23	8	4	+1.2	6553	59	1	2
-40.6	6820	12	4	4	+1.7	6373	56	2	1
-39.3	6818	13	4	4	+1.7	6522	51	2	2
-38.0	6817	18	4	4	+2.3	6358	44	2	1
-36.6	6824	18	4	4	+2.3	6493	48	2	2
-35.3	6824	20	4	4	+3.0	6369	51	2	1
-34.0	6811	33	4	4	+3.0	6497	42	2	2
-32.7	6780	16	4	4	+3.0	6612	17	2	3
-31.4	6765	21	4	4	+3.6	6363	32	2	1
-30.0	6761	28	4	4	+3.6	6469	45	2	2
-28.7	6772	14	4	4	+3.6	6614	13	2	3
-27.4	6778	26	4	4	+4.3	6389	64	2	1
-26.1	6763	28	4	4	+4.3	6468	22	2	2
-24.8	6730	36	4	4	+4.3	6606	34	2	3
-23.4	6730	40	6	4	+5.0	6371	40	2	1
-21.5	6750	33	6	4	+5.0	6462	29	2	2
-19.5	6724	0	6	4	+5.0	6601	21	2	3
-17.5	6728	86	4	4	+5.6	6333	6	4	1
-16.2	6744	27	3	4	+5.6	6403	64	4	2
-15.2	6756	26	3	4	+5.6	6587	13	4	3
-14.2	6740	19	3	4	+6.9	6342	47	3	1
-13.2	6738	11	3	2	+6.9	6438	42	3	2
-13.2	6798	17	3	1	+6.9	6579	17	3	3
-12.2	6783	40	3	4	+8.3	6337	0	2	1
-11.2	6791	28	2	4	+8.3	6386	63	2	2
-10.6	6796	25	2	4	+8.3	6572	18	2	3
-9.9	6794	25	2	4	+9.0	6338	12	3	1
-9.2	6786	25	2	4	+9.0	6382	28	3	2
-8.6	6783	33	2	4	+9.0	6567	16	3	3
-7.9	6759	35	2	2	+9.9	6338	16	3	1
-7.9	6818	14	2	1	+9.9	6364	27	3	2
-7.3	6755	54	2	2	+9.9	6559	15	3	3
-7.3	6813	0	2	1	+10.9	6360	16	3	1
-6.6	6751	60	2	2	+10.9	6367	41	3	2
-6.6	6817	0	2	1	+10.9	6556	26	3	3
-5.9	6710	46	2	2	+12.2	6368	8	3	1
-5.9	6784	40	2	1	+12.2	6374	40	3	2
-5.3	6724	47	2	2	+12.2	6522	42	3	3
-5.3	6798	16	2	1	+13.2	6367	21	3	4
-4.6	6720	30	2	2	+14.2	6361	24	3	4
-4.6	6798	17	2	1	+15.2	6348	21	3	4
-4.0	6711	33	2	2	+16.2	6342	22	3	4
-4.0	6804	12	2	1	+17.2	6332	25	3	4
-3.3	6685	36	2	2	+18.2	6327	25	3	4
-3.3	6813	19	2	1	+19.1	6321	28	3	4
-2.6	6666	37	2	2	+20.1	6317	20	3	4
-2.0	6645	36	2	2	+21.1	6311	25	3	4
-1.3	6633	43	2	2	+22.1	6305	32	3	4
-0.7	6567	89	2	1	+23.1	6305	16	3	4
-0.7	6616	44	2	2	+24.1	6308	12	3	4
0.0	6488	90	2	1	+25.1	6327	30	3	4
0.0	6586	36	2	2	+26.1	6326	39	6	4
+0.7	6360	50	2	1	+28.1	6320	15	6	4
+0.7	6542	70	2	2	+30.0	6361	0	6	4
+1.2	6396	62	1	1					

^a Identification of the gas components: 1, 2, 3 indicate kinematic data referring to component (i), (ii), and (iii) respectively; 4 is used for the gas in the outer regions of the disk.

Table 2. UGC 10205 major axis [N II] kinematics

r	v	σ	n	i^a	r	v	σ	n	i^a
(1)	(2)	(3)	(4)	(5)	(1)	(2)	(3)	(4)	(5)
-42.4	6822	19	8	4	+1.2	6368	46	1	1
-40.4	6829	0	4	4	+1.2	6522	104	1	2
-39.1	6824	11	4	4	+1.7	6376	61	2	1
-37.7	6819	14	4	4	+1.7	6525	59	2	2
-36.4	6822	18	4	4	+2.3	6360	48	2	1
-35.1	6828	20	4	4	+2.3	6475	91	2	2
-33.8	6818	39	4	4	+3.0	6353	32	2	1
-32.4	6784	29	4	4	+3.0	6491	69	2	2
-31.1	6763	35	4	4	+3.6	6367	30	2	1
-29.8	6796	47	4	4	+3.6	6481	34	2	2
-28.5	6784	0	4	4	+3.6	6606	52	2	3
-27.1	6783	3	4	4	+4.3	6365	34	2	1
-25.8	6784	12	4	4	+4.3	6464	27	2	2
-24.5	6729	0	4	4	+4.3	6607	30	2	3
-22.8	6721	0	6	4	+5.0	6369	47	2	1
-20.9	6799	10	6	4	+5.0	6470	23	2	2
-18.9	6736	0	6	4	+5.0	6604	18	2	3
-17.2	6790	99	4	4	+6.0	6377	16	4	1
-16.1	6749	22	3	4	+6.0	6448	97	4	2
-15.1	6755	35	3	4	+6.0	6589	0	4	3
-14.1	6738	6	3	4	+7.1	6337	0	3	1
-13.1	6735	9	3	2	+7.1	6391	26	3	2
-13.1	6789	20	3	1	+7.1	6600	0	3	3
-12.1	6766	50	3	4	+8.3	6345	0	2	1
-11.3	6799	21	2	4	+8.3	6411	13	2	2
-10.6	6802	32	2	4	+8.3	6572	12	2	3
-9.9	6795	19	2	4	+9.1	6348	18	3	1
-9.3	6786	28	2	4	+9.1	6412	44	3	2
-8.6	6783	40	2	4	+9.1	6569	14	3	3
-7.9	6757	39	2	2	+10.1	6351	17	3	1
-7.9	6827	0	2	1	+10.1	6381	26	3	2
-7.3	6747	73	2	2	+10.1	6565	16	3	3
-7.3	6814	0	2	1	+11.1	6362	10	3	1
-6.6	6741	72	2	2	+11.1	6371	39	3	2
-6.6	6818	0	2	1	+11.1	6549	23	3	3
-6.0	6740	55	2	2	+12.4	6370	3	3	1
-5.3	6727	69	2	2	+12.4	6378	37	3	2
-5.3	6810	0	2	1	+12.4	6552	14	3	3
-4.6	6731	57	2	2	+13.4	6369	27	3	4
-4.6	6815	15	2	1	+14.4	6376	20	3	4
-4.0	6711	41	2	2	+15.4	6350	23	3	4
-4.0	6809	6	2	1	+16.4	6345	18	3	4
-3.3	6685	41	2	2	+17.4	6338	28	3	4
-3.3	6810	0	2	1	+18.4	6337	24	3	4
-2.7	6662	46	2	2	+19.4	6324	22	3	4
-2.0	6641	47	2	2	+20.4	6315	18	3	4
-1.3	6613	84	2	2	+21.4	6323	22	3	4
-0.7	6505	144	2	1	+22.3	6306	16	3	4
-0.7	6618	64	2	2	+23.3	6303	24	3	4
0.0	6422	73	2	1	+24.3	6310	26	3	4
0.0	6588	68	2	2	+25.3	6311	0	3	4
+0.7	6393	80	2	1	+26.8	6344	38	6	4
+0.7	6560	78	2	2	+30.8	6353	0	6	4

^a as in Table 1.